

Wavefront Control and Intensity Modulation of Third Harmonic Generation in Nonlocal Metasurfaces

Yu Tian^{1,2}, Nuo Wang¹, Qi Liu^{1,2}, Shuyuan Xiao³, Tingting Liu³, Olivier J. F. Martin⁴, and Ying Gu^{1,2,5,6,7*}

¹State Key Laboratory of Artificial Microstructure and Mesoscopic Physics & Department of Physics, Peking University, Beijing 100871, China

²Frontiers Science Center for Nano-optoelectronics & Collaborative Innovation Center of Quantum Matter & Beijing Academy of Quantum Information Sciences, Peking University, Beijing 100871, China

³School of Information Engineering, Nanchang University, Nanchang 330031, China

⁴Nanophotonics and Metrology Laboratory, Swiss Federal Institute of Technology Lausanne (EPFL), Lausanne CH-1015, Switzerland

⁵Collaborative Innovation Center of Extreme Optics, Shanxi University, Taiyuan, Shanxi 030006, China

⁶Peking University Yangtze Delta Institute of Optoelectronics, Nantong 226010, China

⁷Hefei National Laboratory, Hefei 230088, China

*Email: ygu@pku.edu.cn

Abstract

Metasurfaces have emerged as a promising platform for integrated nonlinear optics. Nonlocal metasurfaces enable high nonlinear conversion efficiency, while the local ones can offer versatile wavefront control, yet achieving both within a single metasurface remains challenging. Here, using a nonlocal phase gradient metasurface, we firstly demonstrate efficient third harmonic generation (THG) with polarization-dependent wavefront control. Leveraging nonlocal nonlinear geometric phase existing at resonance, the third harmonic light with distinct polarizations is deflected into \pm 2nd and \pm 4th diffraction orders, simultaneously achieving a conversion efficiency up to 1.45×10^{-4} under a pump intensity of 1 GW/cm^2 . Then, by introducing a secondary fundamental beam, whose generated third harmonic light overlaps with that of the first beam, the intensity modulation of THG is obtained. The THG efficiency can be tuned from 3.9×10^{-9} to 5.5×10^{-3} by varying the relative phase, polarization and intensity of two fundamental beams. Through utilizing the advantages of both local and nonlocal metasurfaces, our results effectively pave the way to on-chip nonlinear photonic devices and signal processing.

Keywords

nonlocal metasurfaces, quasi bound states in the continuum, third harmonic generation, high conversion efficiency, wavefront control, intensity modulation

Introduction

Metasurfaces, a class of two-dimensional artificial materials, offer exceptional control over amplitude, phase, polarization and other properties of light at the micro/nano scale,^{1–3} enabling various classical and quantum applications.^{4–6} By harnessing near-field enhancement, resonant metasurfaces further facilitate frequency-domain manipulation for nonlinear frequency conversion, which makes them promising candidates for integrated nonlinear optics.^{7–9} To date, a variety of nonlinear processes, including harmonic generation and frequency mixing, have been demonstrated in metasurfaces with plasmonic resonances or Mie modes.^{10–12} For instance, third harmonic generation (THG) has been reported on silicon metasurfaces with conversion efficiencies exceeding $10^{-6} \sim 10^{-5}$, nearly a four-order-of-magnitude enhancement over unpatterned silicon films.^{13–15} Despite these advances, the overall nonlinear conversion efficiencies of these metasurfaces remain relatively low, primarily because they operate under local modes with limited quality factors ($Q < 10^2$). To enhance the conversion efficiency, nonlocal metasurfaces, manifested as strong near-field enhancement and higher quality factors ($Q > 10^3$),^{16,17} have been introduced into nonlinear optics. Among them, metasurfaces supporting quasi-bound states in the continuum (q-BICs) have emerged as an important branch, which can principally provide nearly infinite quality factors through tailoring structural symmetry and geometric perturbations,^{18,19} thereby boosting nonlinear processes.¹⁷ Leveraging q-BICs, silicon metasurfaces have realized highly efficient THG with conversion efficiencies up to 10^{-4} ,^{20–22} corresponding to nearly a two-order-of-magnitude improvement relative to their local-mode counterparts. Beyond THG, nonlocal metasurfaces have also demonstrated higher-order nonlinear processes,^{23,24} as well as quantum nonlinear phenomena like spontaneous parametric down-conversion,^{25,26} all of which disclose their emerging prospects for advanced nonlinear photonics.

Despite the remarkable nonlinear enhancement provided by nonlocal metasurfaces, another key requirement is to simultaneously tailor the wavefront of generated harmonic light. While in local metasurfaces, harmonic wavefront can be readily tailored through independently engineering nonlinear responses of individual unit cells with high precision, facilitating nonlinear diffraction,^{27,28} nonlinear holography,^{29,30} vortex beam generation,³¹ and others. However, achieving nonlinear wavefront control in nonlocal metasurfaces remains challenging, because the response of each unit cell is strongly influenced by that of others, which makes it difficult to engineer the nonlinear response of individual unit cells independently. Recently, nonlocal metasurfaces encoded with geometric phase gradient, termed as nonlocal phase gradient metasurfaces (NPGMs), have been proposed for spectrally selective wavefront manipulation in linear optics.^{32–34} By extending such geometric phase from linear to nonlinear regime, it becomes possible to simultaneously achieve high conversion efficiency and flexible wavefront control on a single NPGM — one of the primary objectives of our research. Furthermore, if established, the capability for nonlinear wavefront control also supports interference among fundamental beams as well as among harmonic light, which offers opportunities for all-optical modulation of nonlinear responses — another objective of our study.

The modulation of harmonic light in nonlinear metasurfaces is vital for signal processing and optical switch.^{35,36} Typically, all-optical modulation is attained by introducing an additional control beam to tune

the refractive index of nonlinear materials, which has been implemented for regulating the conversion efficiencies of second harmonic and third harmonic (TH).^{37–39} Nevertheless, these approaches predominantly rely on third-order nonlinear processes, like Kerr effect and two-photon absorption, whose nonlinear coefficients are remarkably low in many materials, thereby limiting the universality and depth of current modulation methods. Alternatively, all-optical modulation can also be obtained through interference, which tailors the electric field distribution within the nonlinear materials. This strategy has been implemented in conventional optical structures,^{40,41} facilitating modulation without dependence on a specific nonlinear coefficient. However, leveraging interference to regulate conversion efficiencies of nonlinear metasurfaces remains largely unexplored. By exploiting wavefront control capability of the NPGM, we reveal that the THG efficiency can be efficiently modulated by changing incident conditions of the secondary fundamental beam.

Here, we firstly demonstrate efficient THG with wavefront control on a single NPGM. The silicon-based NPGM supports q-BIC with a quality factor of approximately 120 and strong near-field enhancement. Building on this, a THG efficiency up to 1.45×10^{-4} is realized at a pump intensity of 1 GW/cm^2 . More importantly, a nonlocal nonlinear geometric phase can be imparted to THG at q-BIC through tuning the rotation angles of unit cells. This phase amounts to $4\theta\sigma$ under co-polarized condition and $8\theta\sigma$ under cross-polarized condition, which is exactly twice that in local metasurfaces,⁸ where θ denotes the rotation angles of unit cells and $\sigma = +1/-1$ represents the right/left-circularly-polarized (RCP/LCP) fundamental light, respectively. Exploiting our proposed nonlocal nonlinear geometric phase, polarization-dependent wavefront control is implemented. Under RCP fundamental beam incident, the generated TH light is deflected into the +2nd and +4th diffraction orders (Figure 1a), while it will be emitted into -2nd and -4th diffraction orders when the incident light is LCP. Then, by introducing a secondary fundamental beam, whose generated TH light overlaps with that of the primary beam (Figure 1b), the interference between two fundamental beams will strongly modulate the THG efficiency (Figure 1c). With varying relative phase, polarization and intensity, the conversion efficiency can be dynamically tuned from 3.9×10^{-9} to 5.5×10^{-3} , corresponding to

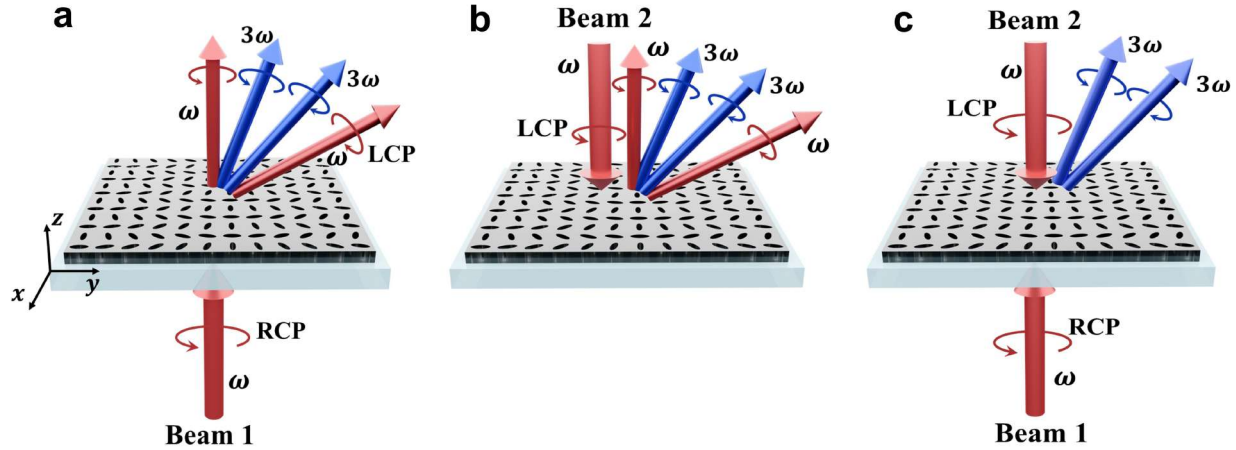


Figure 1: Schematic of wavefront control and intensity modulation of THG on a single NPGM. (a, b) A fundamental beam of (a) RCP light incident from substrate side or (b) LCP light incident from air side is incident into the NPGM. The generated TH light in the air side is deflected into +2nd and +4th diffraction orders. (c) Intensity modulation of THG on the same NPGM when Beam 1 and Beam 2 are incident simultaneously. Their generated TH light overlaps, leading to the modulation of THG efficiency with a near-unity depth.

a near-unity modulation depth. Our results overcome key limitations of the simultaneous realization of high conversion efficiency and flexible wavefront control, which pave the way toward compact and multifunctional nonlinear optical devices. Furthermore, the interference-based modulation of nonlinear conversion efficiency holds promising prospects for on-chip nonlinear signal processing and optical switch.

Results and Discussion

1. Wavefront control of THG in NPGM

Now, we start to investigate efficient THG with wavefront control on the NPGM. Such NPGMs have been reported to tailor the wavefront of linear optical fields, accompanied by strong near-field enhancement.^{32–34} By applying it to the nonlinear optics, it is expected that high conversion efficiency and flexible wavefront manipulation of nonlinear optical fields can be attained on a single NPGM. In this section, we firstly examine the enhanced THG process, whose efficiency is significantly improved compared with that of local metasurfaces.^{13,15} Notably, NPGM also provides the nonlocal nonlinear geometric phase for polarization-dependent wavefront control of TH light only at q-BIC. Therefore, high nonlinear conversion efficiency and versatile wavefront engineering can be simultaneously obtained on a single NPGM, which provides promising

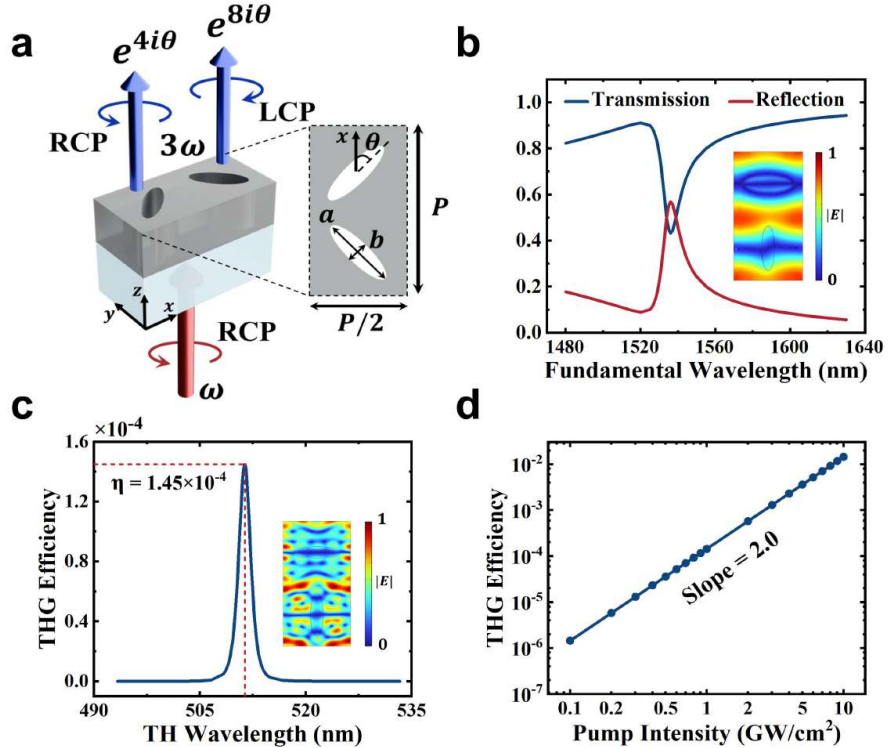


Figure 2: Enhanced THG within the unit cell of NPGM (a) The schematic of THG process in the periodic unit cell. (b) The transmission/reflection spectra of unit cell with its electric field distribution in the xy-plane at q-BIC. (c) The THG efficiency of unit cell as a function of TH wavelength under a pump intensity of 1 GW/cm^2 , with the electric field distribution in the xy-plane at the wavelength of 511.3 nm. (d) The relation of THG efficiency with the pump intensity. Here, a fundamental beam of RCP light is incident into the unit cell normally from substrate.

prospects for on-chip applications of nonlinear metasurfaces.

1.1 Linear and nonlinear responses of unit cell. Consider the periodically arranged unit cell consisted of a silicon slab (gray part) etched with elliptical holes placed on a glass substrate (light blue part), as illustrated in [Figure 2a](#). The refractive index of silicon is taken from experimental data (See Supporting Information Section S1),⁴² while that of glass substrate is fixed as 1.5. The unit cell has a thickness of 260 nm and a period constant of $P = 750$ nm. Besides, the rotation angle of elliptical holes is fixed as $\theta = 0^\circ$ with major axis of $a = 260$ nm and minor axis of $b = 70$ nm. For THG process in silicon unit cells, the nonlinear polarization can be expressed as $\mathbf{P}^{3\omega} = \varepsilon_0 \chi_3 (\mathbf{E}^\omega \cdot \mathbf{E}^\omega) \mathbf{E}^\omega$, where ε_0 is the vacuum permittivity, $\chi_3 = 2.45 \times 10^{-19} \text{ m}^2/\text{V}^2$ is the third-order susceptibility of silicon,⁴³ and \mathbf{E}^ω is the electric field at the fundamental wavelength. Here, the TH conversion efficiency is defined as $\eta = P_{TH}/P_F$, where P_{TH} denotes the TH power radiated from the air side, and P_F refers to the pump power at the fundamental wavelength. The numerical analysis is performed using the finite element method solver in commercial software COMSOL Multiphysics in the frequency domain (further details are included in the Methods section).

We begin by investigating linear and nonlinear responses of the above unit cell. It supports the q-BIC located at 1536 nm with a quality factor of approximately 120, as confirmed by the transmission and reflection spectra in [Figure 2b](#). The q-BIC facilitates strong near-field enhancement within silicon materials (the inset of [Figure 2b](#)), which can be applied to enhance THG process. When the pump beam is RCP with an intensity of 1 GW/cm^2 , the conversion efficiency reaches its peak of 1.45×10^{-4} at the TH wavelength of 511.3 nm ([Figure 2c](#)), representing nearly a two-order-of-magnitude improvement compared to local metasurfaces.^{13–15} Consistent with the preceding discussion, THG predominantly occurs at the position of strong near-field enhancement at q-BIC (the inset of [Figure 2c](#)). Moreover, as the pump intensity increases, the THG efficiency increases linearly with a fitted slope of 2.0 with logarithmic coordinate ([Figure 2d](#)), confirming the characteristics of THG process.²⁸ Additionally, TH light is also emitted from the substrate side, whose intensity is slightly lower than that of air side (See Supporting Information Section S2). Owing to their similar properties, we only focus on the intensity and wavefront of the air-side TH light. Therefore, efficient THG has been implemented at q-BIC with the consideration of unit cell in the NPGM.

1.2 Nonlocal nonlinear geometric phase. In addition to THG enhancement, a nonlocal nonlinear geometric phase can be imparted to TH light. Specifically, when the fundamental beam at q-BIC is incident into unit cells of the NPGM, the RCP and LCP components of generated TH light will carry geometric phases determined by the rotation angle θ of elliptical holes ([Figure 2a](#)). The relations between geometric phase and θ can be analytically obtained from the nonlinear polarization of THG in circularly polarized basis. Taking RCP light incidence as an example, the RCP and LCP components of nonlinear polarization can be expressed as

$$P_R^{3\omega} = e^{i4\theta} \varepsilon_0 \chi_{RRRR} E_R^\omega E_R^\omega E_R^\omega, \quad P_L^{3\omega} = e^{i8\theta} \varepsilon_0 \chi_{LRRR} E_R^\omega E_R^\omega E_R^\omega, \quad (1)$$

where χ_{LRRR} refers to the nonlinear coefficient that enables three RCP photons at frequency ω to generate one LCP photon at frequency 3ω . As a result, when a beam of RCP light at q-BIC is incident into the unit cell with a rotation angle of θ , the LCP component of TH light carries a phase of 8θ , while RCP component carries a phase of 4θ ([Figure 2a](#)). Conversely, when the incident light is LCP, the LCP component of TH light carries a phase of -4θ , and the RCP component carries a phase of -8θ (see Supporting Information Section S3 for detailed derivation).

The above analysis about nonlocal nonlinear geometric phase can be verified through simulations. We first construct 12 types of unit cells with a relative rotation angle of 15° . These unit cells are the same in

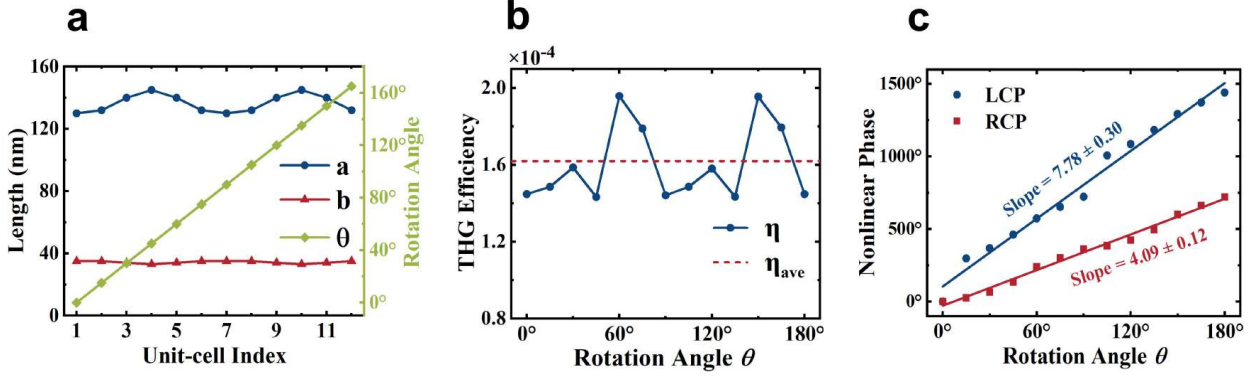


Figure 3: (a) The geometric parameters of unit cells in the NPGM. The major and minor axes of elliptical holes are adjusted with rotation angles to maintain the same q-BIC wavelength and similar THG efficiencies. (b) The THG efficiency and (c) nonlinear geometric phase of periodic unit cells with varying rotation angles. Here, the fundamental beam is RCP light with an intensity of 1 GW/cm^2 to generate TH light of 511.3 nm.

period constant and thickness, but the major axis a and minor axis b of their elliptical holes are adjusted with rotation angles accordingly (Figure 3a). This is to ensure all unit cells support the same wavelength of q-BIC as well as comparable THG efficiencies, as illustrated in Figure 3b. Only under these conditions, the far-field distribution of TH light is solely determined by the nonlocal nonlinear geometric phase encoded by unit cells, thereby allowing nonlinear wavefront manipulation. Then, the relations between nonlinear geometric phases of TH light and rotation angles θ are calculated. Under RCP light illumination at the q-BIC, when the rotation angles of unit cell changes by θ , the nonlinear phase of RCP component of TH light varies by 4θ , and that of LCP component changes by 8θ (Figure 3c), which are consistent with the above analytical results in Eq. (1). For LCP fundamental beam incidence, the conditions are similar. Therefore, the nonlocal nonlinear geometric phase is well established, which is the foundation of nonlinear wavefront engineering in the NPGM.

Notably, the proposed nonlocal nonlinear geometric phase is distinct from the previously reported nonlinear geometric phase in local metasurfaces in terms of response amplitude and operating bandwidth.^{8, 27, 30, 44, 45} Typically, for linear/nonlinear processes in local metasurfaces, the geometric phases are $(n - 1)\theta\sigma$ and $(n + 1)\theta\sigma$ for co-polarization and cross-polarization conditions, respectively,⁸ where n refers to the order of nonlinear processes, θ denotes the rotation angle of unit cells and $\sigma = +1/-1$ represents RCP/LCP fundamental beam. For linear process ($n = 1$), they are 0 and $2\theta\sigma$ for co-polarization and cross-polarization conditions, respectively,³ for THG process ($n = 3$), they are $2\theta\sigma$ for co-polarization condition and $4\theta\sigma$ for cross-polarization condition.³⁰ These are established by the fact that when the rotation angle of unit cell of local metasurfaces changes by θ , the principal axis also rotates by θ accordingly. However, for the unit cell in nonlocal phase gradient metasurfaces, a rotation by θ leads to a 2θ rotation of its principal axis.³² As a result, the geometric phases for linear optical fields are 0 and $4\theta\sigma$ under co and cross-polarization conditions, respectively,^{33, 34} which are twice those in local metasurfaces. Accordingly, the nonlocal nonlinear geometric phases for THG process are also twice those of local metasurfaces, which are $4\theta\sigma$ and $8\theta\sigma$ under co and cross-polarization conditions. These are also confirmed by the above analytical results in Eq. (1) and simulations. Moreover, in contrast to the broadband responses in local metasurfaces,^{8, 44} the nonlinear geometric phase in the NPGM only exists at q-BIC. Thus, the nonlocal nonlinear geometric phase enables the NPGM to engineer the wavefront of TH light at q-BIC.

1.3 Wavefront control of THG. To manipulate the wavefront of TH light, we firstly construct the NPGM composed of the above 12 types of unit cells (Figure 1a). It supports the q-BIC located at 1529 nm with transmission and reflection spectra displayed in Figure 4a, which exhibits a slight blueshift relative to the condition of single-unit-cell periodic arrangement.³²⁻³⁴ There is strong near-field enhancement within silicon materials at q-BIC (the inset of Figure 4a), thereby boosting the THG process. As a result, when the incident fundamental beam is RCP with an intensity of 1 GW/cm^2 , the THG efficiency exceeds $\eta = 1.45 \times 10^{-4}$ at the TH wavelength of 509 nm, as illustrated in Figure 4b. Compared with local metasurfaces with phase gradients,²⁹⁻³¹ this is an improvement of more than two orders of magnitude. Meanwhile, the intensity of TH light emitting from substrate side is relatively lower than that of air side (See Supporting Information Section S2). Therefore, by exploiting the NPGM, highly efficient THG process can be implemented at the q-BIC.

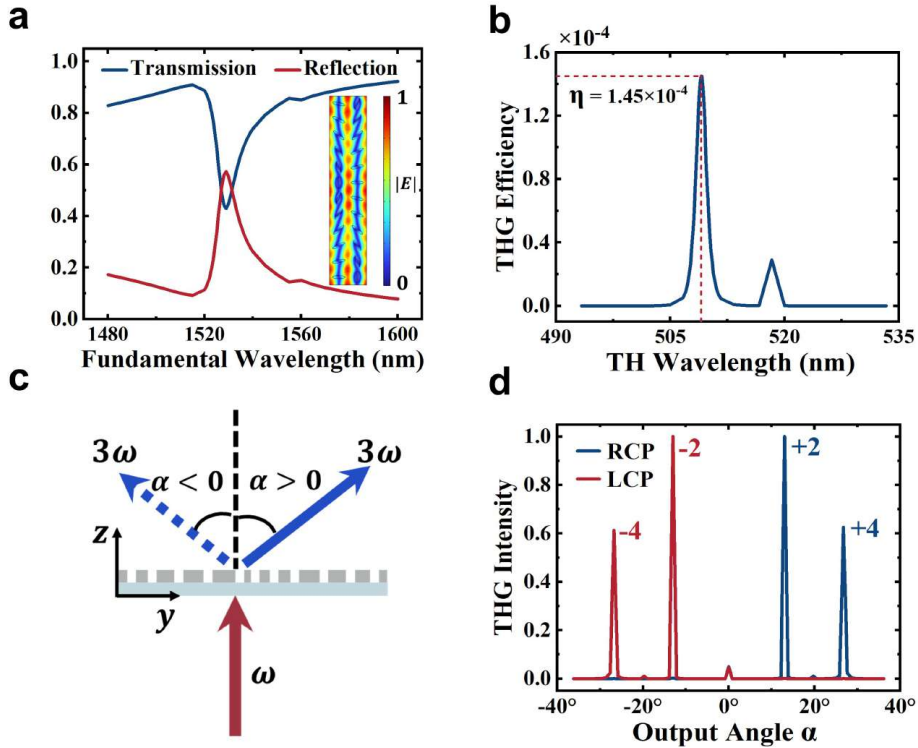


Figure 4: (a) The transmission/reflection spectra of NPGM with electric field distribution in the xy-plane at q-BIC. (b) The THG efficiency of NPGM as a function of TH wavelength. (c) The schematic of output angle α of TH light. (d) The distribution of normalized THG intensity with RCP and LCP fundamental beams incidence from substrate side normally.

While enhancing THG efficiency, polarization-dependent wavefront control of TH light can be achieved at q-BIC. The THG intensity distribution among output angle α can be obtained through Fourier transform (See details in the Methods Section), where α is defined as the angle between the emission direction of TH light and $+z$ axis (Figure 4c). As illustrated in Figure 4d, with RCP fundamental beam incidence, the output angles of TH light are mainly $\alpha = 13.1^\circ$ and 26.9° , corresponding to the $+2$ nd and $+4$ th diffraction orders at the wavelength of 509 nm, respectively. This nonlinear wavefront control originates from the nonlocal nonlinear geometric phases discussed above. According to Eq. (1) and numerical results in Figure 3c, the phases of TH light for co and cross-polarization conditions in the NPGM are $+4\theta$ and $+8\theta$, respectively,

indicating that the TH light will output from + 2nd and + 4th diffraction orders, which is in good agreement with the numerical results in [Figure 4d](#). Meanwhile, the fundamental beam mainly outputs from directions with output angles of 0° and 42.7° , corresponding to the 0th and + 2nd diffraction orders at the wavelength of 1527 nm (see Supporting Information Section S4), which are also consistent with the reported geometric phases of 0 and 4θ for linear optical fields.³²⁻³⁴ In contrast, when the incident fundamental light is LCP, the TH light is primarily emitted into – 2nd and – 4th diffraction orders ([Figure 4d](#)). For fundamental beam with other polarizations, since it can be regarded as the superposition of RCP and LCP light, its TH light will output from the \pm 2nd and \pm 4th diffraction orders, simultaneously. Thus, in the NPGM, the wavefront of TH light can be tailored at q-BIC with polarization-dependent and spectrally selective characteristics.

In a word, we have demonstrated highly efficient THG with polarization-dependent wavefront manipulation at q-BIC on a single NPGM, overcoming key limitations of the simultaneous realization of high conversion efficiency and wavefront control in nonlinear metasurfaces. Building on these, more flexible wavefront control can be realized through NPGMs by designing nonlocal nonlinear geometric phase gradients. So it is expected that NPGM can facilitate more advanced functionalities, such as nonlinear holography^{29,30} and vortex beam generation,³¹ which are essential for versatile nonlinear light sources. In contrast to local metasurfaces with broadband responses,^{8,44} NPGMs possess inherently narrowband phase responses. This allows spectrally selective wavefront engineering of nonlinear optical fields to promote the development of multifunctional nonlinear photonic devices. Beyond classical nonlinear optics, the NPGM can also be extended to facilitate quantum nonlinear processes accompanied by wavefront control, including spontaneous parametric down-conversion and four-wave mixing, which offers opportunities for the generation and manipulation of quantum states with larger entanglement and efficiency. The wavefront control capability of the NPGM also provide possibilities for intensity modulation of THG via interference, which we will discuss in the following section.

2. Intensity Modulation of THG

Here, we intend to investigate the intensity-modulation of THG via interference in the same NPGM. The discussions in previous section are focused on passive nonlinear responses with fixed functionalities once fabricated. All-optical modulation is crucial for on-demand applications of the NPGM, which can be realized through the interference between two fundamental beams. In this section, based on the polarization-dependent wavefront control for TH light, a secondary fundamental beam is introduced, whose TH light overlaps with that of the first fundamental beam ([Figure 1b](#)). By inputting these two fundamental beams simultaneously ([Figure 1c](#)), the THG efficiency can be tuned from 3.9×10^{-9} to 5.5×10^{-3} by adjusting the relative phase, intensity and polarization. The interference-based modulation of THG exhibits a near-unity modulation depth, which can be applied in all-optical switch and nonlinear signal processing.

2.1 The mechanism for intensity modulation. We first elucidate the physical mechanism governing the modulation of THG efficiency through interference between two fundamental beams. When only the first fundamental beam is incident, the induced electric field distribution in the NPGM is denoted as $\mathbf{E}_1^\omega = (E_{1x}, E_{1y}, E_{1z})^T$, whose specific form is determined by its phase, intensity and polarization. When only the second fundamental beam illuminates the NPGM, the induced electric field distribution is referred as $\mathbf{E}_2^\omega = (E_{2x}, E_{2y}, E_{2z})^T$. If these two fundamental beams are incident simultaneously, the total electric field distribution in the NPGM becomes the coherent superposition of \mathbf{E}_1^ω and \mathbf{E}_2^ω , expressed as $\mathbf{E}_s^\omega = \mathbf{E}_1^\omega + \mathbf{E}_2^\omega = (E_{1x} + E_{2x}, E_{1y} + E_{2y}, E_{1z} + E_{2z})^T$. Accordingly, the nonlinear polarization for THG in the NPGM is given

by

$$\mathbf{P}_s^{3\omega} = \epsilon_0 \chi_3 (\mathbf{E}_s^\omega \cdot \mathbf{E}_s^\omega) \mathbf{E}_s^\omega, \quad (2)$$

where ϵ_0 is the vacuum permittivity, $\chi_3 = 2.45 \times 10^{-19} \text{ m}^2/\text{V}^2$ is the third-order susceptibility of silicon.⁴³ So, the THG efficiency is determined by the total electric field distribution \mathbf{E}_s^ω formed through the interference between two fundamental beams. By varying the incident conditions of secondary fundamental beam, \mathbf{E}_s^ω can be substantially tailored, thereby facilitating efficient modulation of THG efficiency. Therefore, the effective interference between two fundamental beams can support the intensity modulation of THG.

In the NPGM, the effective interference occurs with overlapping of TH light generated by two fundamental beams, as schematically illustrated in Figure 1. As discussed in the previous section, for the RCP/LCP fundamental beam incidence from substrate side, the TH light is predominantly emitted into $+2\text{nd}/-2\text{nd}$ and $+4\text{th}/-4\text{th}$ diffraction orders. Conversely, when RCP/LCP fundamental light is incident from air side, the TH light primarily outputs from $-2\text{nd}/+2\text{nd}$ and $-4\text{th}/+4\text{th}$ diffraction orders. Considering these, we fix the first fundamental beam (Beam 1) as RCP light incidence from substrate side with an intensity of 1 GW/cm^2 , while the second fundamental beam (Beam 2) is incident from air side with varying phase, intensity and polarization. Under this configuration, when Beam 2 is LCP, strong interference occurs, since its generated TH light overlaps with that produced by Beam 1 (Figure 1c). When Beam 2 is RCP, the interference will almost disappear. Consequently, by varying the phase, intensity and polarization of Beam 2, the intensity modulation of THG can be obtained in the same NPGM.

2.2 The demonstration of intensity modulation. By adjusting the phase of Beam 2, the THG efficiency can be manipulated with a near-unity modulation depth. Here, Beam 2 is RCP or LCP light with an intensity of 1 GW/cm^2 and a relative phase $\Delta\varphi$ with respect to Beam 1, where $\Delta\varphi$ is defined as the difference in propagation phases between Beam 1 and Beam 2, namely, $\Delta\varphi = \varphi_1 - \varphi_2$ (the inset of Figure 5b). As shown in Figure 5a, when Beam 2 is LCP, the THG efficiency can be tuned from 3.9×10^{-9} to 5.5×10^{-3} , spanning over six orders of magnitude. This represents a near-unity modulation depth, which is superior to existing results relying on Kerr effect and two-photon absorption.³⁷⁻³⁹ Notably, the THG efficiency is minimum at $\Delta\varphi = 0^\circ$, while it is maximum at $\Delta\varphi = 180^\circ$. This is due to the coupling coefficient between q-BIC and Beam 1 is opposite to that of Beam 2 (see Supporting Information Section S5). When Beam 2 is RCP, the relation between THG efficiency and $\Delta\varphi$ is completely different. As $\Delta\varphi$ is varied, the THG efficiency remains nearly constant, as shown by the red curve in Figure 5a. This is because the generated TH light from the two fundamental beams has nearly no overlap, leading to the absence of interference. Therefore, the intensity modulation of THG in the NPGM can be achieved by changing the phase of Beam 2 of LCP.

Then, based on this, we explore the modulation of THG efficiency by varying the intensity of Beam 2 with LCP state (Figure 5b). As the intensity of Beam 2 increases at $\Delta\varphi = 0^\circ$, the THG efficiency initially decreases and then increases, with a minimum efficiency of $\eta = 1.1 \times 10^{-10}$ under an intensity of 1.4 GW/cm^2 . This behavior results from destructive interference between two fundamental beams, which has $|\mathbf{E}_s^\omega| = ||\mathbf{E}_1^\omega| - |\mathbf{E}_2^\omega||$. In contrast, as the intensity of Beam 2 increases at $\Delta\varphi = 180^\circ$, the THG efficiency increases continuously, since the two beams are under constructive interference, namely, $|\mathbf{E}_s^\omega| = ||\mathbf{E}_1^\omega| + |\mathbf{E}_2^\omega||$. Thus, by properly adjusting the intensity of Beam 2, we can also engineer the THG efficiency in the NPGM.

Furthermore, we systematically analyze influences of the polarization of Beam 2 on THG efficiency. For

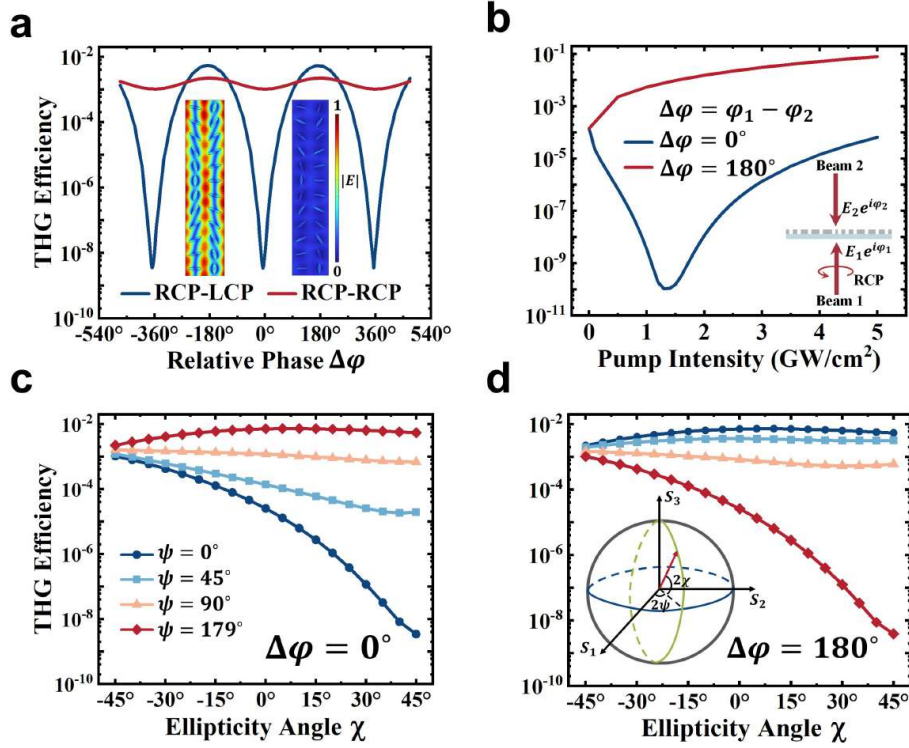


Figure 5: The intensity modulation of THG efficiency through varying (a) relative phase $\Delta\varphi$, (b) pump intensity of Beam 2, and polarization of Beam 2 with (c) $\Delta\varphi = 0^\circ$ and (d) $\Delta\varphi = 180^\circ$. The insets in (a) are the electric field distribution of fundamental beam in the xy-plane at $\Delta\varphi = 180^\circ$ (left) and $\Delta\varphi = 0^\circ$ (right), which exhibits large near-field enhancement under constructive interference, while approaches zero under destructive interference. The inset in (d) is the physical meanings of orientation angle ψ and ellipticity angle χ on the Poincaré sphere.

Beam 2 propagating along the -z axis, its Jones vector can be written as

$$\begin{bmatrix} E_x \\ E_y \end{bmatrix} = \begin{bmatrix} \cos \chi \cos \psi - i \sin \chi \sin \psi \\ \cos \chi \sin \psi + i \sin \chi \cos \psi \end{bmatrix}, \quad (3)$$

where $\psi \in [0^\circ, 180^\circ]$ is the orientation angle, and $\chi \in [-45^\circ, 45^\circ]$ is the ellipticity angle. When $\chi = 45^\circ$ and -45° , it corresponds to LCP and RCP states with Jones vectors of $|L_-\rangle = 1/\sqrt{2} [1, i]^T$ and $|R_-\rangle = 1/\sqrt{2} [1, -i]^T$, respectively. When $\chi = 0^\circ$, it represents linear polarization, while other values of χ correspond to elliptical polarization. For Beam 2 with arbitrary polarization $|a\rangle$, it can be decomposed into RCP and LCP components as $|a\rangle = m|R_-\rangle + n|L_-\rangle$, where the coefficients are given by $m = \cos(\chi + 45^\circ)e^{i\psi}$ and $n = \sin(\chi + 45^\circ)e^{-i\psi}$, satisfying $|m|^2 + |n|^2 = 1$. The amplitudes and phases of coefficients m and n can be adjusted by varying orientation angle ψ and ellipticity angle χ . According to the above discussion, the LCP component of Beam 2 can effectively interfere with Beam 1, whereas the RCP component does not contribute to the interference. Therefore, the coefficient n of LCP component of Beam 2 can be modulated by adjusting its polarization, thereby modulating the THG efficiency, as illustrated in Figure 5c,d.

When the initial relative phase is $\Delta\varphi = 0^\circ$, destructive interference occurs between Beam 1 and Beam 2, leading to the minimum THG efficiency. As illustrated in Figure 5c, the THG efficiency reaches its

minimum value of $\eta = 3.9 \times 10^{-9}$ with $\psi = 0^\circ, \chi = 45^\circ$, corresponding to Beam 2 as LCP light with an additional phase of 0° . Conversely, the THG efficiency peaks at $\eta = 5.3 \times 10^{-3}$ when $\psi = 179^\circ, \chi = 45^\circ$, corresponding to Beam 2 as LCP light with an additional phase of 179° . If χ takes other values, the THG efficiency increases with orientation angle ψ . This is because under these conditions, the amplitude of LCP component coefficient n remains constant, while its phase gradually increases with ψ , shifting from destructive interference to constructive interference. On the other hand, when ψ is fixed, an increase in χ leads to a larger amplitude of LCP component, which results in a decrease in THG efficiency for $\psi < 90^\circ$ (destructive interference), and an increase for $\psi > 90^\circ$ (constructive interference). Thus, the THG efficiency, spanning over six orders of magnitude, exhibits remarkable sensitivity to the polarization of Beam 2, enabling polarization-controlled intensity switch with a near-unity modulation depth. When the initial relative phase is $\Delta\varphi = 180^\circ$, constructive interference occurs between Beam 1 and Beam 2, leading to the maximum THG efficiency. As illustrated in [Figure 5d](#), the polarization-dependent modulation is exact opposite of that observed for $\Delta\varphi = 0^\circ$ in [Figure 5c](#). The THG efficiency peaks at $\eta = 5.5 \times 10^{-3}$ for $\psi = 0^\circ, \chi = 45^\circ$, while it reaches its minimum value of $\eta = 3.5 \times 10^{-9}$ at $\psi = 179^\circ, \chi = 45^\circ$, also spanning over six orders of magnitude. Therefore, we demonstrate near-unity modulation of THG efficiency through adjusting the polarization of Beam 2, which holds significant potential for applications in polarization-controlled switch in nonlinear optics.

Conclusions

In conclusion, we have achieved an efficient THG process with polarization-dependent wavefront control on a single NPGM, and further demonstrated the intensity switch of THG. By exploiting q-BIC, the THG efficiency of the silicon-based NPGM exceeds 10^{-4} under a pump intensity of 1 GW/cm^2 , representing an enhancement of nearly two orders of magnitude relative to local metasurfaces. Simultaneously, nonlocal nonlinear geometric phase can be obtained at q-BIC for polarization-dependent wavefront control for TH light. Furthermore, through introducing a secondary fundamental beam, intensity switch of THG is achieved via linear interference. The THG efficiency can be dynamically tuned from 10^{-9} to 10^{-3} by adjusting the relative phase, intensity and polarization of the second beam, spanning over six orders of magnitude with a near-unity modulation depth. These results address a fundamental challenge in nonlinear metasurfaces, which is to realize high conversion efficiency and flexible wavefront control simultaneously, thereby providing a viable route toward multifunctional nonlinear optical devices. Moreover, the demonstrated interference-based, near-unity modulation of nonlinear conversion efficiency highlights the potential of this platform for nonlinear optical switch and on-chip signal processing.

Methods

Numerical simulation

The linear and nonlinear responses of the NPGM is calculated through COMSOL Multiphysics. The general simulation model is an infinite periodic surface consisted with a silicon slab with elliptical holes placed on a glass substrate, as shown in [Figure 1](#) and [Figure 2](#). The periodicity of structure is modeled by introducing periodic boundary conditions along x and y directions. In the top and bottom surface of the model, perfect match layer (PML) are applied for open boundary conditions. The periodic ports are utilized to serve as

the input optical fields propagating along $+z$ or $-z$ directions. The refractive index of amorphous silicon is taken from experimental date considering the dispersion and dissipation,⁴² which is displayed in the Supporting Information Section S1, while those of substrate and air are fixed as 1.5 and 1.0, respectively. In simulations, the THG is taken into account through the nonlinear polarization $\mathbf{P}^{3\omega} = \epsilon_0 \chi_3 (\mathbf{E}^\omega \cdot \mathbf{E}^\omega) \mathbf{E}^\omega$, where $\chi_3 = 2.45 \times 10^{-19} \text{ m}^2/\text{V}^2$ is obtained through experimental data.⁴³ During this process, the backward frequency conversion is neglected. Therefore, two frequency-domain solvers are required in the calculations, which correspond to the fundamental and TH wavelengths, respectively. The optical field distribution obtained by the first solver serve as the input of the second solver. For the second solver, continuous boundary conditions are performed along x and y directions, while PML condition is used along z direction. Then, the surface integral of TH light power flux over the top and bottom surfaces of model can be conducted to measure the output power of TH light. To measure the output angles of TH light, Fourier transform is performed through COMSOL Multiphysics. An $x-y$ cross-section sufficiently far from the NPGM is obtained and then replicated along x and y directions to acquire the far field distribution of TH light in the spatial domain. Then, perform the Fourier transform on it and extract the data corresponding to $k_x = 0$.

Supporting information

Notes

The authors declare no competing financial interest.

Acknowledgements

This work is supported by the National Natural Science Foundation of China under Grant No. U25D9003 and No. 12474370 and the Quantum Science and Technology-National Science and Technology Major Project No. 2021ZD0301500.

References

- [1] Yu, N.; Genevet, P.; Kats, M. A.; Aieta, F.; Tetienne, J.-P.; Capasso, F.; Gaburro, Z. Light Propagation with Phase Discontinuities: Generalized Laws of Reflection and Refraction. *Science* **2011**, *334* (6054), 333–337.
- [2] Chen, H.-T.; Taylor, A. J.; Yu, N. A Review of Metasurfaces: Physics and Applications. *Rep. Prog. Phys.* **2016**, *79* (7), 076401.
- [3] Liu, Q.; Liu, X.; Tian, Y.; Tian, Z.; Li, G.; Ren, X.-F.; Gong, Q.; Gu, Y. Parallel Beam Splitting Based on Gradient Metasurface: From Classical to Quantum. *Opt. Express* **2024**, *32* (18), 31389–31404.
- [4] Stav, T.; Faerman, A.; Maguid, E.; Oren, D.; Kleiner, V.; Hasman, E.; Segev, M. Quantum Entanglement of the Spin and Orbital Angular Momentum of Photons Using Metamaterials. *Science* **2018**, *361* (6407), 1101–1104.
- [5] Liu, Q.; Liu, X.; Tian, Y.; Tian, Z.; Li, G.; Ren, X.-F.; Gong, Q.; Gu, Y. Multiphoton Path-Polarization Entanglement through a Single Gradient Metasurface. *Adv. Photonics Nexus* **2025**, *4* (2), 026002.

[6] Liu, Q.; Tian, Y.; Tian, Z.; Jia, Y.; Li, G.; Ren, X.-F.; Gong, Q.; Gu, Y. Quantum CZ Gates on a Single Gradient Metasurface. *Light Sci. Appl.* **2025**, *14* (1), 193.

[7] Lee, J.; Tymchenko, M.; Argyropoulos, C.; Chen, P.-Y.; Lu, F.; Demmerle, F.; Boehm, G.; Amann, M.-C.; Alù, A.; Belkin, M. A. Giant Nonlinear Response from Plasmonic Metasurfaces Coupled to Intersubband Transitions. *Nature* **2014**, *511* (7507), 65–69.

[8] Li, G.; Zhang, S.; Zentgraf, T. Nonlinear Photonic Metasurfaces. *Nat. Rev. Mater.* **2017**, *2* (5), 1–14.

[9] Grinblat, G. Nonlinear Dielectric Nanoantennas and Metasurfaces: Frequency Conversion and Wavefront Control. *ACS Photonics* **2021**, *8* (12), 3406–3432.

[10] Liu, S.; Sinclair, M. B.; Saravi, S.; Keeler, G. A.; Yang, Y.; Reno, J.; Peake, G. M.; Setzpfandt, F.; Staude, I.; Pertsch, T.; Brener, I. Resonantly Enhanced Second-Harmonic Generation Using III–V Semiconductor All-Dielectric Metasurfaces. *Nano Lett.* **2016**, *16* (9), 5426–5432.

[11] Liu, S.; Vabishchevich, P. P.; Vaskin, A.; Reno, J. L.; Keeler, G. A.; Sinclair, M. B.; Staude, I.; Brener, I. An All-Dielectric Metasurface as a Broadband Optical Frequency Mixer. *Nat. Commun.* **2018**, *9* (1), 2507.

[12] Celebrano, M.; Wu, X.; Baselli, M.; Großmann, S.; Biagioni, P.; Locatelli, A.; De Angelis, C.; Cerullo, G.; Osellame, R.; Hecht, B.; Duò, L.; Ciccacci, F.; Finazzi, M. Mode Matching in Multiresonant Plasmonic Nanoantennas for Enhanced Second Harmonic Generation. *Nat. Nanotechnol.* **2015**, *10* (5), 412–417.

[13] Shcherbakov, M. R.; Neshev, D. N.; Hopkins, B.; Shorokhov, A. S.; Staude, I.; Melik-Gaykazyan, E. V.; Decker, M.; Ezhov, A. A.; Miroshnichenko, A. E.; Brener, I.; Fedyanin, A. A.; Kivshar, Y. S. Enhanced Third-Harmonic Generation in Silicon Nanoparticles Driven by Magnetic Response. *Nano Lett.* **2014**, *14* (11), 6488–6492.

[14] Yang, Y.; Wang, W.; Boulesbaa, A.; Kravchenko, I. I.; Briggs, D. P.; Puretzky, A.; Geohegan, D.; Valentine, J. Nonlinear Fano-Resonant Dielectric Metasurfaces. *Nano Lett.* **2015**, *15* (11), 7388–7393.

[15] Grinblat, G.; Li, Y.; Nielsen, M. P.; Oulton, R. F.; Maier, S. A. Efficient Third Harmonic Generation and Nonlinear Subwavelength Imaging at a Higher-Order Anapole Mode in a Single Germanium Nanodisk. *ACS Nano* **2017**, *11* (1), 953–960.

[16] Kolkowski, R.; Hakala, T. K.; Shevchenko, A.; Huttunen, M. J. Nonlinear Nonlocal Metasurfaces. *Appl. Phys. Lett.* **2023**, *122* (16), 160502.

[17] Vabishchevich, P.; Kivshar, Y. Nonlinear Photonics with Metasurfaces. *Photonics Res.* **2023**, *11* (2), B50–B64.

[18] Hsu, C. W.; Zhen, B.; Stone, A. D.; Joannopoulos, J. D.; Soljačić, M. Bound States in the Continuum. *Nat. Rev. Mater.* **2016**, *1* (9), 1–13.

[19] Koshelev, K.; Lepeshov, S.; Liu, M.; Bogdanov, A.; Kivshar, Y. Asymmetric Metasurfaces with High-Q Resonances Governed by Bound States in the Continuum. *Phys. Rev. Lett.* **2018**, *121* (19), 193903.

[20] Liu, Z.; Xu, Y.; Lin, Y.; Xiang, J.; Feng, T.; Cao, Q.; Li, J.; Lan, S.; Liu, J. High-Q Quasi bound States in the Continuum for Nonlinear Metasurfaces. *Phys. Rev. Lett.* **2019**, *123* (25).

[21] Xiao, S.; Qin, M.; Duan, J.; Liu, T. Robust Enhancement of High-Harmonic Generation from All-Dielectric Metasurfaces Enabled by Polarization-Insensitive Bound States in the Continuum. *Opt. Express* **2022**, *30* (18), 32590–32599.

[22] Liu, T.; Qin, M.; Qiu, J.; Tu, X.; Qiu, H.; Wu, F.; Yu, T.; Liu, Q.; Xiao, S. Polarization-Independent Enhancement of Third-Harmonic Generation Empowered by Doubly Degenerate Quasi-Bound States in the Continuum. *Nano Lett* **2025**, *25* (9), 3646–3652.

[23] Carletti, L.; Kruk, S. S.; Bogdanov, A. A.; De Angelis, C.; Kivshar, Y. High-Harmonic Generation at the Nanoscale Boosted by Bound States in the Continuum. *Phys. Rev. Res.* **2019**, *1* (2), 023016.

[24] Zograf, G.; Koshelev, K.; Zalogina, A.; Korolev, V.; Hollinger, R.; Choi, D.-Y.; Zuerch, M.; Spielmann, C.; Luther-Davies, B.; Kartashov, D.; Makarov, S. V.; Kruk, S. S.; Kivshar, Y. High-Harmonic Generation from Resonant Dielectric Metasurfaces Empowered by Bound States in the Continuum. *ACS Photonics* **2022**, *9* (2), 567–574.

[25] Parry, M.; Mazzanti, A.; Poddubny, A. N.; Valle, G. D.; Neshev, D. N.; Sukhorukov, A. A. Enhanced Generation of Nondegenerate Photon Pairs in Nonlinear Metasurfaces. *Adv. Photonics* **2021**, *3* (5), 055001.

[26] Santiago-Cruz, T.; Gennaro, S. D.; Mitrofanov, O.; Addamane, S.; Reno, J.; Brener, I.; Chekhova, M. V. Resonant Metasurfaces for Generating Complex Quantum States. *Science* **2022**, *377* (6609), 991–995.

[27] Bar-David, J.; Levy, U. Nonlinear Diffraction in Asymmetric Dielectric Metasurfaces. *Nano Lett.* **2019**, *19* (2), 1044–1051.

[28] Hail, C. U.; Michaeli, L.; Atwater, H. A. Third Harmonic Generation Enhancement and Wavefront Control Using a Local High-Q Metasurface. *Nano Lett.* **2024**, *24* (7), 2257–2263.

[29] Gao, Y.; Fan, Y.; Wang, Y.; Yang, W.; Song, Q.; Xiao, S. Nonlinear Holographic All-Dielectric Metasurfaces. *Nano Lett.* **2018**, *18* (12), 8054–8061.

[30] Reineke, B.; Sain, B.; Zhao, R.; Carletti, L.; Liu, B.; Huang, L.; De Angelis, C.; Zentgraf, T. Silicon Metasurfaces for Third Harmonic Geometric Phase Manipulation and Multiplexed Holography. *Nano Lett.* **2019**, *19* (9), 6585–6591.

[31] Wang, L.; Kruk, S.; Koshelev, K.; Kravchenko, I.; Luther-Davies, B.; Kivshar, Y. Nonlinear Wavefront Control with All-Dielectric Metasurfaces. *Nano Lett.* **2018**, *18* (6), 3978–3984.

[32] Overvig, A. C.; Malek, S. C.; Carter, M. J.; Shrestha, S.; Yu, N. Selection Rules for Quasibound States in the Continuum. *Phys. Rev. B* **2020**, *102* (3), 035434.

[33] Overvig, A. C.; Malek, S. C.; Yu, N. Multifunctional Nonlocal Metasurfaces. *Phys. Rev. Lett.* **2020**, *125* (1), 017402.

[34] Overvig, A.; Alù, A. Wavefront-Selective Fano Resonant Metasurfaces. *Adv. Photonics* **2021**, *3* (2), 026002.

[35] Sain, B.; Meier, C.; Zentgraf, T. Nonlinear Optics in All-Dielectric Nanoantennas and Metasurfaces: A Review. *Adv. Photonics* **2019**, *1* (2), 024002.

[36] Maiuri, M.; Schirato, A.; Cerullo, G.; Della Valle, G. Ultrafast All-Optical Metasurfaces: Challenges and New Frontiers. *ACS Photonics* **2024**, *11* (8), 2888–2905.

[37] Sartorello, G.; Olivier, N.; Zhang, J.; Yue, W.; Gosztola, D. J.; Wiederrecht, G. P.; Wurtz, G.; Zayats, A. V. Ultrafast Optical Modulation of Second- and Third-Harmonic Generation from Cut-Disk-Based Metasurfaces. *ACS Photonics* **2016**, *3* (8), 1517–1522.

[38] Pogna, E. A. A.; Celebrano, M.; Mazzanti, A.; Ghirardini, L.; Carletti, L.; Marino, G.; Schirato, A.; Viola, D.; Laporta, P.; De Angelis, C.; Leo, G.; Cerullo, G.; Finazzi, M.; Della Valle, G. Ultrafast, All Optically Reconfigurable, Nonlinear Nanoantenna. *ACS Nano* **2021**, *15* (7), 11150–11157.

[39] Bijloo, F.; Murzyn, K.; van Emmerik, F.; den Boef, A. J.; Kraus, P. M.; Koenderink, A. F. Near-Unity All-Optical Modulation of Third-Harmonic Generation with a Fano-Resonant Dielectric Metasurface. *Nano Lett.* **2024**, *24* (41), 12942–12947.

[40] Hareli, L. On-the-Fly Control of High-Harmonic Generation Using a Structured Pump Beam. *Phys. Rev. Lett.* **2018**, *120* (18).

[41] Li, W.-Z. Creating Multibeam Interference from Two-Beam Interference with the Assistance of Harmonics Generation. *Phys. Rev. Res.* **2025**, *7* (2).

[42] Palik, E. D. *Handbook of Optical Constants of Solids*; Academic Press, 1985.

[43] Hon, N. K.; Soref, R.; Jalali, B. The Third-Order Nonlinear Optical Coefficients of Si, Ge, and $\text{Si}_{1-x}\text{Ge}_x$ in the Midwave and Longwave Infrared. *J. Appl. Phys.* **2011**, *110* (1), 011301.

[44] Liu, B.; Sain, B.; Reineke, B.; Zhao, R.; Meier, C.; Huang, L.; Jiang, Y.; Zentgraf, T. Nonlinear Wavefront Control by Geometric-Phase Dielectric Metasurfaces: Influence of Mode Field and Rotational Symmetry. *Adv. Opt. Mater.* **2020**, *8* (9), 1902050.

[45] Reineke Matsudo, B.; Sain, B.; Carletti, L.; Zhang, X.; Gao, W.; de Angelis, C.; Huang, L.; Zentgraf, T. Efficient Frequency Conversion with Geometric Phase Control in Optical Metasurfaces. *Adv. Sci.* **2022**, *9* (12), 2104508.